# Synthesis and *ab initio* calculations of nanolaminated $(Cr,Mn)_2AlC$ compounds

Aurelija Mockute,[1] Martin Dahlqvist,[1] Jens Emmerlich,[2] Lars Hultman,[1] Jochen M. Schneider,[2]
Per O. Å. Persson,[1] and Johanna Rosen[1]

[1]*Thin Film Physics, Department of Physics, Chemistry, and Biology (IFM), Linköping University, SE-58183 Linköping, Sweden*
[2]*Materials Chemistry, RWTH-Aachen, D-52074 Aachen, Germany*

(Received 28 June 2012; published 26 March 2013)

We present an *ab initio* theoretical analysis of the temperature-dependent stability of inherently nanolaminated $(Cr_{1-x}Mn_x)_2AlC$. The results indicate energetic stability over the composition range $x = 0.0$ to 0.5 for temperatures $\geqslant$600 K. Corresponding thin film compounds were grown by magnetron sputtering from four elemental targets. X-ray diffraction in combination with analytical transmission electron microscopy, including electron energy-loss spectroscopy and energy dispersive x-ray spectroscopy analysis, revealed that the films were epitaxial (0001)-oriented single-crystals with $x$ up to 0.16.

DOI: 10.1103/PhysRevB.87.094113 PACS number(s): 81.15.Cd, 68.37.Lp, 79.20.Uv, 31.15.A−

MAX phases constitute a family of inherently nanolaminated compounds with a general composition of $M_{n+1}AX_n$, where M denotes an early transition metal, A is an A-group element, and X is C and/or N.[1] Presence of both metallic and covalent bonds between different layers provides a unique combination of metallic and ceramic properties, such as high (anisotropic) conductivity, hardness, and thermal shock resistance.[2] Fascinating MAX phase phenomena range from extreme damage tolerance including reversible deformation[3] over oxidation induced self-healing behavior[4] to stability of nanosheets upon exfoliation.[5] More than 60 phases have been synthesized to date,[6] and we have only seen the beginning of their significance in applications.

The MAX phase properties can be further improved by alloying, e.g., $(Ti_{0.8}V_{0.2})_2AlC$ exhibits enhancement of Vickers hardness, flexural strength, and shear strength by 29%, 26%, and 45%, respectively, compared to $Ti_2AlC$. However, the substituting elements are generally chosen from those used in previously synthesized MAX phases, exemplified in $(Ti,V,Nb,Cr)_2AlC$,[7,8] $Ti_3(Si,Al,Ge,Sn)C_2$,[9,10] and $Ti_2Al(C,N)$.[11] M, A, and X elements outside conventional compositions are likely to provide more pronounced changes in the properties, or even new characteristics. Promising candidates are those neighboring the already known M, A, and X elements, due to similar atom size and electronic structure. One such example is substitution of C in $Ti_2AlC$ with up to 13 at.% of O,[12,13] which is an exchange of approximately half of the X atoms in the structure. The latter work was motivated by a theoretical study suggesting a tunable anisotropic conductivity in $Ti_2AlC_xO_y$.[14] Besides substitution of M, A, or X elements the addition of interstitial elements may also be useful for the materials design of MAX phases. Recently the incorporation of interstitial oxygen in $Cr_2AlC$ was reported.[15] This incorporation may be of relevance during the initial stages of oxidation and hence self-healing of $Cr_2AlC$.

An approach for predicting phase stability of hypothetical and not yet synthesized MAX phases has previously been developed.[16,17] With this approach, the most recent study predicts $(Cr_{1-x}Mn_x)_2AlC$ as a new magnetic nanoscale laminate, with a ferromagnetic (FM) or antiferromagnetic (AFM) state dependent on the Cr-Mn atomic configuration on the MAX phase M site.[18] To date, no MAX phase including Mn has been synthesized, and hence, these results motivate experimental investigations on stability of $Cr_2AlC$ upon substitution of Cr by Mn.

In this paper we report experimental evidence for a new Mn-containing MAX phase compound, employing analytical transmission electron microscopy (TEM). The presented observations of a $(Cr_{1-x}Mn_x)_2AlC$ MAX phase are accompanied by atomistic calculations on phase stability and structural changes upon Mn incorporation, with results consistent with the experimental findings.

Based on experimental conditions of simultaneous deposition flux of Cr and Mn, a random Cr-Mn intermixing on the M site in $(Cr_{1-x}Mn_x)_2AlC$ is expected. Using *ab initio* calculations based on density functional theory (DFT), we have therefore performed total energy calculations of disordered M-element configurations in $(Cr_{1-x}Mn_x)_2AlC$, in order to mimic a solid solution of Cr and Mn. This is modeled using a methodology for creating so-called special quasirandom structures (SQS),[19] introduced by Zunger *et al.* and later used also for MAX phases.[16] Two different supercell sizes, $4 \times 2 \times 1$ and $2 \times 2 \times 2$ unit cells, were used for $(Cr_{1-x}Mn_x)_2AlC$ with $x = 0.25$ and 0.50, each supercell containing 32 M sites. For further details of calculation parameters see Ref. 18.

Based on the previously developed theoretical approach for predicting the phase stability of compounds and alloys within higher order materials systems,[17] we have calculated the formation enthalpy $\Delta H_{cp}$ of $(Cr_{1-x}Mn_x)_2AlC$ relative to its identified most stable competing phases (cp) $Cr_2AlC$, $Mn_3AlC$, MnAl, and C.[18] The result corresponds to the top curve (0 K) in Fig. 1(a), which is above zero for $x > 0$. Hence, at 0 K the chemically disordered alloy can be concluded unstable with respect to decomposition into competing phases. However, due to the random distribution of Cr and Mn on the M site, it is possible to estimate the phase stability in terms of Gibbs free energy $\Delta G_{cp}$ by introducing the effect of configurational entropy $\Delta G_{cp} = \Delta H_{cp} - TS$, where $\Delta H_{cp}$ is the formation enthalpy at 0 K and $T$ is the temperature. $S$ is the configurational entropy given by $-2k_B[x \ln x + (1-x)\ln(1-x)]$, where $k_B$ is the Boltzmann constant and $x$ corresponds to the amount of Mn on the M site. With $S$ being $>0$, $\Delta G_{cp}$ decreases with increasing $T$, and thus stabilizes $(Cr_{1-x}Mn_x)_2AlC$. Figure 1(a) indicates phase stability around

 

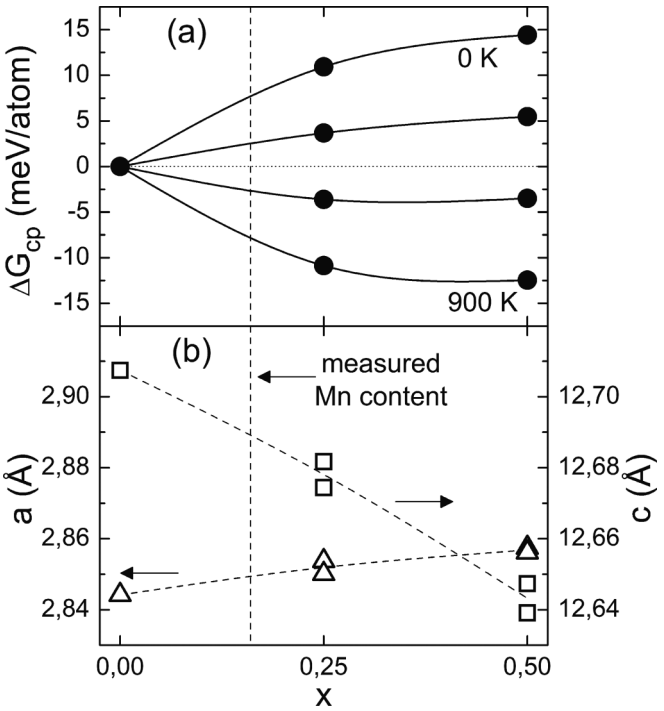


FIG. 1. (a) $\Delta G_{cp} = \Delta H_{cp} - TS$ for $(Cr_{1-x}Mn_x)_2AlC$ from 0 to 900 K, in steps of 300 K. (b) Lattice parameters $a$ and $c$ for $(Cr_{1-x}Mn_x)_2AlC$ for two different SQS supercells. The curves act as a guide for the eye, and represent average values of the two supercells.

600 K and above, with $\Delta G_{cp}$ being negative for all $x$ considered. Based on this analysis, materials synthesis has not been attempted below 300 °C.

As the Mn incorporation into $Cr_2AlC$ increases, the lattice parameters may change. In Fig. 1(b) the calculated values for $a$ and $c$ are shown for both supercells used. The dashed curves serve as a guide for the eye, and represent the average value of the two cells. As the Mn content $x$ increases, the $c$ axis decreases almost linearly, accompanied with a minute change in $a$. However, it should be noted that $c$ is dependent on the magnetic configuration simulated, with a resulting change in $c$ with increasing $x$ around, or lower than, the changes shown in the figure. According to the graph, a Mn incorporation of 12.5 at.% ($x = 0.25$) would be accompanied by a reduction in $c$ of about 0.03 Å as compared to $Cr_2AlC$, which would correspond to a 0.03° peak shift for the (0002) peak in an XRD scan. However, considering possible peak shift due to, e.g., growth induced stress in the film, the extent of Mn incorporation in the MAX phase structure cannot be safely concluded based on XRD analysis alone.

$(Cr,Mn)_2AlC$ films were deposited on $Al_2O_3(0001)$ substrates using dc magnetron sputtering from four elemental targets. Prior to deposition the substrates were degassed in the vacuum chamber at the growth temperature of 600 °C for 10 min. The vacuum chamber had a base pressure of $9.4 \times 10^{-9}$ Torr, and during film growth Ar was introduced to a partial pressure of $2.5 \times 10^{-3}$ Torr. The depositions were carried out with power densities at 2.0, 1.5, 2.5, and 7.6 W/cm$^2$ for the Cr, Mn, Al, and C targets, respectively, at a sample-target distance of 10 cm. Deposition time of 1 h resulted in a film thickness of ~1 $\mu$m.

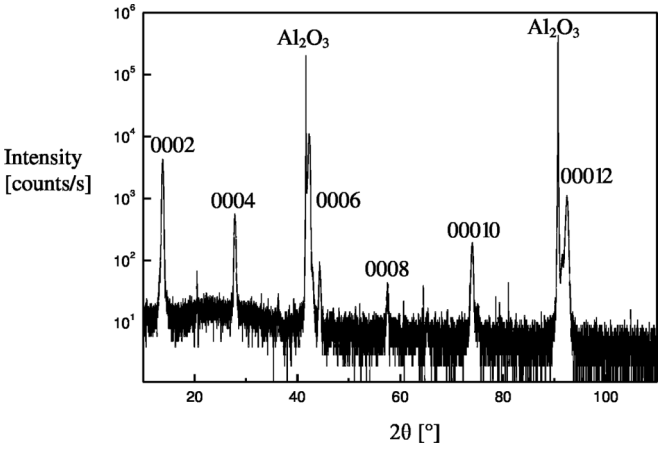


FIG. 2. $\theta$-$2\theta$ XRD scan from a $(Cr_{1-x}Mn_x)_2AlC$ film deposited on $Al_2O_3(0001)$. An extra peak at 44.4° originates from CrMn.

X-ray diffraction (XRD) measurements were performed for phase identification using a Panalytical Empyrian MRD equipped with a line focus Cu$K_\alpha$ source. A hybrid mirror and a 0.27° collimator were used on the incident and diffracted beam side, respectively. A diffractogram from XRD $\theta$-$2\theta$ analysis is shown in Fig. 2. Based on the identified peaks, the film consists predominantly of epitaxially oriented 211 MAX phase, with the peak locations and $c$-lattice parameter of 12.8 Å, calculated from the Braggs law, being consistent with $Cr_2AlC$. As discussed in connection to Fig. 1(b), no significant shift in peak positions is expected as a result of Mn incorporation. A CrMn peak at 44.4° and a few unidentified peaks of intensity close to noise level can be found in the diffractogram. These peaks, together with expected grain boundaries and lattice defects within the film, allow nonlocal composition analysis to be used only as indication of the actual MAX phase composition. Hence, analytical TEM is used for quantification of Mn content in areas of high-quality MAX-phase structure.

A cross-sectional sample for TEM analysis was prepared by conventional mechanical methods followed by low-angle Ar-ion milling with a final fine-polishing step at low acceleration voltage. Imaging and spectrum mapping were employed in a Tecnai G2 TF20 UT FEG instrument operated at 200 kV. High resolution scanning TEM (HRSTEM) was performed in the doubly corrected Linköping FEI Titan[3] 60-300. The TEM analysis reveals large (≫100 nm) grains of high crystal quality. Figure 3(a) shows an overview of a MAX phase grain, which grows all the way from the substrate, and in (b) the lattice resolved image [from the upper right corner of (a)] confirms the epitaxial nature of the film. The bright field (S)TEM image in Fig. 3(c) from the same region of the sample indicates the area employed for spectrum imaging by energy dispersive x-ray (EDX-SI) and electron energy-loss spectroscopy (EELS-SI). While EELS has a finer dispersion than EDX, the mapped spectral features are of lower energy. Hence, the A element (Al-K) was mapped by EDX and the X element (C-K) by EELS. Furthermore, different lines of Cr and Mn were mapped by EDX and EELS, respectively. This is beneficial as the mapped Mn-$K_{\alpha1,\alpha2}$ overlap with Cr-$K_{\beta1}$ in the EDX spectrum, but with EELS, the Cr-$L_{2,3}$ and Mn-$L_{2,3}$ edges are separated. Strong signals from all four elements are found in this MAX phase

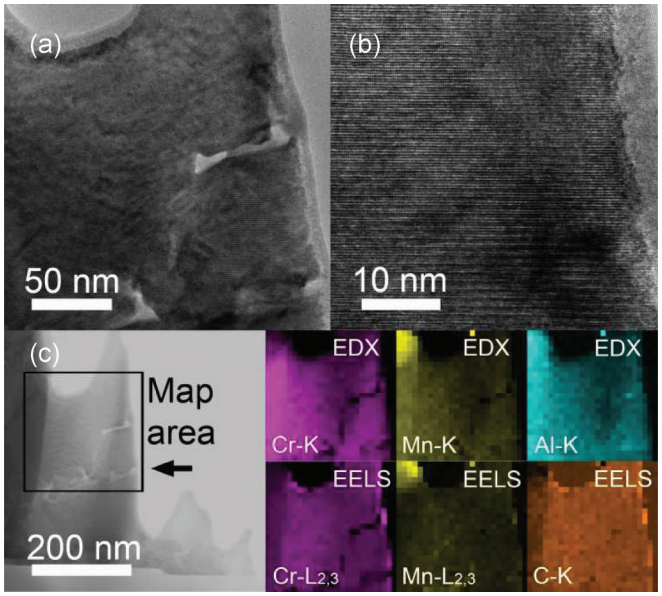


FIG. 3. (Color online) (a) Overview and (b) high-resolution TEM images of the $(Cr_{1-x}Mn_x)_2AlC$ film and (c) corresponding elemental distributions obtained by EDX and EELS.

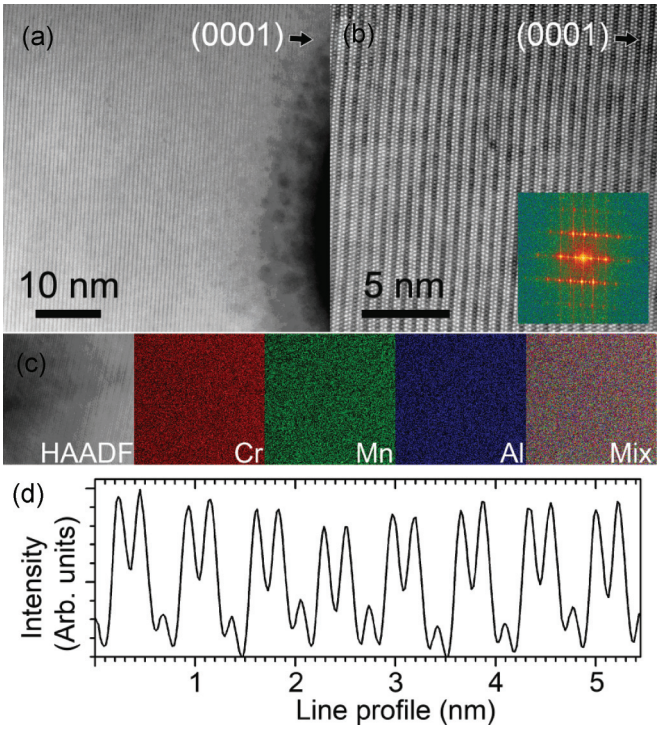


FIG. 4. (Color online) (a) Lattice resolved and (b) high resolution HAADF-STEM images of the $(Cr_{1-x}Mn_x)_2AlC$ film with (c) corresponding high magnification elemental distributions obtained by EDX and (d) integrated HAADF-STEM line profile [from (b)].

structure, indicating a compound incorporating Mn. The Mn concentration was further quantified by both EDX and EELS at ∼8 at.%, assuming a relative M element concentration of 50 at.% in the MAX phase (Cr ∼42 at.%). This assumption can be based on a high formation energy for M-site vacancies, observed in, for example, $Ti_2AlC$.[20] C and Al were estimated close to the ideal stoichiometric values, ∼25 at.% (23 and 28 at.%, respectively). Note also, that the elemental mapping indicates a homogeneous film composition consistent with a single-phase material, as seen in Fig. 3.

To further investigate the homogeneity of the film, HRSTEM imaging and mapping of the sample were performed as shown in Fig. 4. The images were recorded from the area under the "(a)" in Fig. 3(a). The image in Fig. 4(a) shows a relatively large and lattice resolved area of the sample. It can be seen that the contrast appears as homogeneous, indicating that the material is uniform with no segregation, by coherent or incoherent inclusions, respectively. Some minor fluctuations in contrast are seen, but these are interpreted as amorphous material on the sample surface which becomes more noticeable towards the sample edge. The higher magnification image in Fig. 4(b) shows the laminated layering and zigzag appearance of a MAX structure, and further in the fast Fourier transform (FFT) [Fig. 4(b) inset]. To investigate the elemental homogeneity of this area, a subarea of Fig. 4(b) was mapped as shown in Fig. 4(c). The cumulative (approximately 5 min) HAADF-STEM image exhibits signs of drift. The drift appears in the image when the beam is deflected by accumulating charges on the sample which cannot be dissipated due to the insulating substrate. As a consequence, lattice resolved elemental images were not achieved. However, the lattice is partly resolved in the HAADF-STEM image, which indicates the level of resolution in the corresponding elemental maps of Cr, Mn, and Al [red, green, and blue colors in Fig. 4(c), respectively]. It is found that all elements are present in this confined area, and that segregation is not present. A line profile from Fig. 4(b) is finally shown in Fig. 4(d). Intensity variations in the double peaks would indicate a separation along the *c* axis of Cr and Mn by consequence of the mass dependent contrast. As can be seen from the profile the intensity is nearly identical and variations appear in both directions. Hence, the Cr and Mn elements can be concluded to assume a random arrangement.

Based on the EELS and EDX analysis it is possible to incorporate at least 8 at.% Mn into $Cr_2AlC$ MAX phase, as indicated by a vertical dashed line in Fig. 1. Considering the theoretical analysis, which is based on configurational entropy to account for the effect of temperature, an even higher Mn concentration can be expected. However, it should be noted that at elevated temperatures thermal entropy effects come into play, which affect the experimentally achievable amount of incorporated Mn.

MAX phase synthesis is often attempted at temperatures above those used in the present investigation. However, previous materials synthesis of fcc Fe-Mn[21] has shown a Mn sticking coefficient close to zero at elevated temperatures, and hence competing effects need to be considered; increasing the temperature to optimize the MAX phase quality, while restraining the temperature in order to maximize the Mn incorporation. When temperatures above 600 °C were used in the present study, no Mn was detected in the films, likely due to evaporation. The solution may be process optimization to deposit the ideal MAX phase stoichiometry, allowing only higher bond strength MAX phase to be formed, hindering Mn evaporation at temperatures above 600 °C.

The study by Dahlqvist *et al.*[18] predicts ferromagnetic properties of a disordered $(Cr_{0.5}Mn_{0.5})_2AlC$ solid solution. The here synthesized $(Cr_{0.84}Mn_{0.16})_2AlC$ films that are (0001) textured and virtually single-phase MAX material is a first important step towards such experiments. Furthermore, the above presented results show the strength of recently developed theory for predicting new MAX phase materials,[16,17] also including elements besides those used previously.

In conclusion, based on predictions from *ab initio* theory of a new stable MAX-phase compound, we have synthesized thin films of nanolaminated $(Cr_{1-x}Mn_x)_2AlC$. The Mn is found to be incorporated into the known MAX phase structure to a concentration of approximately 8 at.% ($x = 0.16$), which according to previously published theoretical work should result in magnetic characteristics.

The research leading to these results has received funding from the European Research Council under the European Community's Seventh Framework Programme (FP7/2007-2013)/ERC Grant agreements No. [258509] and No. [227754], the Knut and Alice Wallenberg Foundation, and the Swedish Research Council (VR) for project and Linnaeus Environment grants. The calculations were carried out using supercomputer resources provided by the Swedish National Infrastructure for Computing (SNIC). J.M.S. acknowledges financial support from DFG-SPP 1299.

[1] H. Nowotny, Prog. Solid State Chem. **2**, 27 (1970).
[2] M. W. Barsoum, Prog. Solid State Chem. **28**, 201 (2000).
[3] M. W. Barsoum, T. Zhen, S. R. Kalidindi, M. Radovic, and A. Murugaiah, Nat. Mater. **2**, 107 (2003).
[4] G. M. Song, Y. T. Pei, W. G. Sloof, S. B. Li, J. T. M. De Hosson, and S. van der Zwaag, Scr. Mater. **58**, 13 (2008).
[5] M. Naguib, M. Kurtoglu, V. Presser, J. Lu, J. Niu, M. Heon, L. Hultman, Y. Gogotsi, and M. W. Barsoum, Adv. Mater. **23**, 4207 (2011).
[6] P. Eklund, M. Beckers, U. Jansson, H. Högberg, and L. Hultman, Thin Solid Films **518**, 1851 (2010).
[7] J. C. Schuster, V. H. Nowotny, and C. Vaccaro, J. Solid State Chem. **32**, 213 (1980).
[8] M. W. Barsoum, I. Salama, T. El-Raghy, J. Golczewski, H. J. Seifert, F. Aldinger, W. D. Porter, and H. Wang, Metall. Mater. Trans. A **33**, 2775 (2002).
[9] B. Manoun, S. K. Saxena, G. Hug, A. Ganguly, E. N. Hoffman, and M. W. Barsoum, J. Appl. Phys. **101**, 113523 (2007).
[10] H. Yang, B. Manoun, R. T. Downs, A. Ganguly, and M. W. Barsoum, J. Phys. Chem. Solids **67**, 2512 (2006).
[11] M. W. Barsoum, T. El-Raghy, and M. Ali, Metall. Mater. Trans. A **31**, 1857 (2000).
[12] P. O. Å. Persson, J. Rosen, D. R. McKenzie, and M. M. M. Bilek, Phys. Rev. B **80**, 092102 (2009).
[13] A. Mockute, M. Dahlqvist, L. Hultman, P. O. Å. Persson, and J. Rosen, J. Mater. Sci. **48**, 3686 (2013).
[14] J. Rosen, M. Dahlqvist, S. I. Simak, D. R. McKenzie, and M. M. M. Bilek, Appl. Phys. Lett. **97**, 073103 (2010).
[15] M. Baben, L. Shang, J. Emmerlich, and J. M. Schneider, Acta Mater. **60**, 4810 (2012).
[16] M. Dahlqvist, B. Alling, I. A. Abrikosov, and J. Rosen, Phys. Rev. B **81**, 024111 (2010).
[17] M. Dahlqvist, B. Alling, and J. Rosen, Phys. Rev. B **81**, 220102(R) (2010).
[18] M. Dahlqvist, B. Alling, I. A. Abrikosov, and J. Rosen, Phys. Rev. B **84**, 220403 (2011).
[19] A. Zunger, S.-H. Wei, L. G. Ferreira, and J. E. Bernard, Phys. Rev. Lett. **65**, 353 (1990).
[20] T. Liao, J. Wang, and Y. Zhou, Scr. Mater. **59**, 854 (2008).
[21] T. Gebhardt, D. Music, M. Ekholm, I. A. Abrikosov, J. von Appen, R. Dronskowski, D. Wagner, J. Mayer, and J. M. Schneider, Acta Mater. **59**, 1493 (2011).